Axisymmetric Nonlinear Waves and Structures in Hall Plasmas

Tanim Islam
Massachusetts Institute of Technology
77 Massachusetts Avenue
Cambridge, MA 02139[*]

Leonid Rudakov
Berkeley Scholars
Springfield, VA[†]
(Dated: May 27, 2003)

A Hall plasma consists of a plasma with not all species frozen into the magnetic field. In this paper, a general equation for the evolution of an axisymmetric magnetic field in a Hall plasma is derived, with an integral similar to the Grad-Shafranov equation. Special solutions arising from curvature – whistler drift modes that propagate along the electron drift as a Burger's shock, and nonlinear periodic and soliton-like solutions to the generalized Grad-Shafranov integral – are analyzed.

We derive analytical and numerical solutions in an electron-ion Hall plasma, in which electrons and ions are the only species in the plasmas. Results may then be applied to electron-ion-gas Hall plasmas, in which the ions are coupled to the motion of gases in low ionized plasmas (lower ionosphere and protostellar disks), and to dusty Hall plasmas (such as molecular clouds), in which the much heavier charged dust may be collisionally coupled to the gas.

PACS numbers: Valid PACS appear here
Keywords: suggested keywords here

I. INTRODUCTION

Hall physics is relevant in plasmas in which one or more species of a plasma are nonmagnetized, such as in laboratory plasmas on time scales much shorter than the inverse ion cyclotron frequency[1–5]. Within the past fifteen years there have been numerous theoretical, experimental, and numerical studies of Hall effects in plasmas. Research, such as that shown in have focused on planar rather than more complicated geometries.

Whistler drift modes propagate as a shock wave via density gradients in a Hall plasma [1] and is a phenomenon applied in plasma opening switches (see e.g. [3, 5, 6] for discussions of Hall physics in plasma opening switches). However, the same drift modes, which propagate as shocks, and whistler-like modes with periodicity, may also be seen when considering curvature effects in the absence of density gradients. More recently, whistler-like modes with curvature effects have been shown to be important in magnetic reconnection in the earth's magnetotail[7]. A linear study of Hall physics in a low-ionized, high-density protostellar disk[8] (i.e. cylindrical geometry) have shown that the whistler frequency is also an important parameter in the stability of the rotating disk. A recent paper by Rudakov has analyzed whistler and whistler drift modes with planar geometry in astrophysical dusty plasmas [9]. This paper analyzes the nonlinear axisymmetric structure of whistler and whistler drift modes.

[*]Electronic address: tanim@mit.edu
[†]Electronic address: rudakovl@wam.umd.edu

A. Magnetodynamic Equation for Electron-Ion Hall Plasmas

The simplest studies of Hall physics consider a two-species plasma in which the electrons are magnetized and the ions are unmagnetized:

$$\omega_{ce}^{-1} \ll \tau \ll \omega_{ci}^{-1} \text{ or } \rho_e \ll \boldsymbol{x} \ll \rho_i \tag{1}$$

Where $\omega_{ce} = eB/m_e c$ is the electron cyclotron frequency, $\omega_{ci} = eB/m_i c$ is the ion cyclotron frequency, $\rho_e = v_{th,e}/\omega_{ce}$ is the electron Larmor radius, and $\rho_i = v_{th,i}/\omega_{ci}$ is the ion Larmor radius. τ and $\boldsymbol{x}$ are the time and length scale of the phenomenon, respectively.

We may then ignore ion velocity $\mathbf{v}_i$ evolution.

$$\frac{dn_e}{dt} = -n_e \nabla \cdot \mathbf{v}_e \tag{2}$$

$$m_e n_e \frac{d\mathbf{v}_e}{dt} = -en_e \left(\mathbf{E} + \frac{1}{c}\mathbf{v}_e \times \mathbf{B} \right) - \nabla P_e - m_e n_e \nu_{ei} \mathbf{v}_e \tag{3}$$

Where $\mathbf{v}_e$ is the electron flow velocity, $\mathbf{v}_g$ is the gas flow velocity, and P_e is the electron pressure. m_e is the electron mass, and ν_{ei} is the electron-ion momentum transfer rate.

The plasma is quasineutral, so $n_e = n_i = n$, where n_e and n_i are electron and ion number densities. For the sake of simplicity, we consider the frequency of this Hall phenomenon to be slow enough as to ignore the electron inertial term relative to the collisional terms. Eq. (3)

then reduces to the following:

$$\begin{aligned}\mathbf{E}+\frac{1}{c}\mathbf{v}_e\times\mathbf{B}&=-\frac{\nabla P_e}{en}+\frac{m_e\nu_{ei}}{e^2n}\mathbf{J}\\ \nabla\times\mathbf{B}&=\frac{4\pi}{c}\mathbf{J}=-\frac{4\pi en}{c}\mathbf{v}_e\end{aligned}\tag{4}$$

Where $\mathbf{J}\approx -en\mathbf{v}_e$. Assume electron pressure $P_e\equiv P_e(n)$. If we take the curl of Eq. (4), and note the continuity equation for electrons (Eq. [2]), then we get the magnetic frozen-in equation which describes the evolution of magnetic fields in an electron-ion Hall plasma:

$$\begin{aligned}&n\frac{\partial}{\partial t}\left(\frac{\mathbf{B}}{n}\right)+n\mathbf{v}_e\cdot\nabla\left(\frac{\mathbf{B}}{n}\right)=\mathbf{B}\cdot\mathbf{v}_e+\\ &\nabla\times\left(\mathcal{D}_M\nabla\times\mathbf{B}\right)\end{aligned}\tag{5}$$

With magnetic diffusion coeffcient $\mathcal{D}_M$ given by the following:

$$\mathcal{D}_M=\frac{m_e\nu_{ei}c^2}{4\pi e^2n}\tag{6}$$

The important point to be made here is that with Hall MHD, compared to the usual MHD, the convection term $\mathbf{B}\cdot\mathbf{v}_e$ is associated with the electron flow rather than the bulk flow of the plasma. Since magnetic fields flow with the electron fluid, we may get penetration of the magnetic field into the bulk medium – a process that is not possible in MHD. Furthermore, for this traditional Hall plasma, one gets the following normalizations: 1) the frequency of Hall phenomena are normalized in units of ω_{ci}; 2) length scales are normalized in units of $d_i=c/\omega_{pi}$, the ion inertial skin depth, where $\omega_{pi}^2=4\pi e^2n/m_i$ is the ion plasma frequency; and 3) velocities of Hall magnetic structures in units of v_A, where $v_A=B_0/\sqrt{4\pi nm_i}$ is the Alfvén velocity. In the Hall limit, if the magnetic field convection, with velocity $\mathbf{v}_e=c\left(\nabla\times\mathbf{B}\right)/(4\pi en)$, is greater than Alfven velocity. This holds if $v_e/v_A\approx c/\left(\omega_{pe}L\right)>1$, where L is the dimensions of the problem. Therefore, the limit $v_i\to 0$ is also often denoted as electron MHD.

B. Low Ionized Hall Plasmas

In low ionized plasmas, the plasma ambipolar drift through the gas under the frozen-in magnetic field pressure is dominant under low ion-gas collision frequencies. But, in the limit $\nu_{ig}\gg\omega_{ci}$ (where ν_{ig} is the ion-gas collision rate and ω_{ci} is the ion cyclotron frequency), ambipolar diffusion should be taken into account as well as the Hall term ($\mathbf{v}_e\times\mathbf{B}=-(\mathbf{J}\times\mathbf{B})/en$) in Eq. (4). Furthermore, if the following condition is met – $\nu_{ei}\nu_{eg}\gg\omega_{ci}\omega_{ce}$ – then ambipolar diffusion is negligible compared to collisional diffusion processes, where here ν_{eg} is the electron-gas collision frequency, and ω_{ce} is the electron cyclotron frequency.

In low-ionized plasmas with ion-gas coupling, we perform the following normalizations: 1) we replace ν_{ei} with ν_{eg} in Eq. (6) provided that ambipolar diffusion is negligible compared to collision diffusion; 2) the ions are coupled to the gas, so that the Alfvén velocity is calculated over the density of gas particles $v_{Ag}=B_0/\sqrt{4\pi m_gn_g}$, where m_g and n_g are the averaged molecular mass and number density of gas particles, respectively; and 3) since Hall plasma time scales are normalized with respect to the ion cyclotron frequency, the Hall length scale (the largest length scale over which we can observe Hall effects) is given by the following:

$$\ell\sim\frac{v_{Ag}}{\omega_{ci}}\approx\frac{c}{\omega_{pi}}\left(\frac{m_g}{m_i}\right)^{1/2}\left(\frac{n_g}{n_i}\right)^{1/2}\tag{7}$$

Furthermore, the collision rates for electrons and ions are given in [10, 11], where A is the molecular/atomic mass of the principal ion:

$$\begin{aligned}\nu_{ig}=&n_g\left\langle\sigma v\right\rangle_{ig}\\ =&2.6\times10^{-9}\left(\frac{A}{1\text{amu}}\right)^{-1/2}\ \text{s}^{-1}\end{aligned}\tag{8}$$

$$\begin{aligned}\nu_{eg}=&n_g\left\langle\sigma v\right\rangle_{eg}\\ =&8.28\times10^{-10}\left(\frac{T}{1K}\right)^{1/2}\ \text{s}^{-1}\end{aligned}\tag{9}$$

In a typical protostellar disk, $n_g\sim10^{12}-10^{13}$ cm^{-3} [12] and magnetic fields of order 10 - 100 mG (see [13] for scaling of magnetic fields in molecular clouds) so that we have Hall plasma. Most of the ions in low-ionized astrophysical plasmas are alkali ions[12, 14], giving an ion mass $m_i\sim30$. For $T\sim30$K, gas density $n_g=10^{13}$ cm^{-3}, assuming a standard cosmic-ray ionization $\zeta=10^{-17}$ s^{-1}[15], ion density $n_i\sim1$ cm^{-3} [16, 17]. Here $\nu_{ig}\sim1.4\times10^5$ cm^{-3}. For $B=100$ mG, $\omega_{ci}=30$ s$^{-1}\ll\nu_{ig}$. Furthermore, $\nu_{ei}=2.6\times10^4$ s^{-1} and $\omega_{ce}=1.8\times10^6$ s^{-1}, so that $\nu_{eg}\nu_{ig}\gg\omega_{ci}\omega_{ce}$, so that we may completely neglect ambipolar diffusion. The upper threshold for Hall effects $L\sim5$ AU (7.5×10^{13} cm), comparable to the scale of temperature and density gradients in the outer parts of a protostellar disk.

For the lowest levels of Earth's ionosphere, the D and E regions (from 70 - 150 km), the atmosphere is mostly N_2 and O_2 with densities of 10^{14} cm^{-3} at 80 km, exponentially decreasing with a scale height of 6 km. In the D region, the ion and electron number density scales as $n_e=200\exp\left((h-70\text{ km})/4.8\text{ km}\right)$ cm^{-3} up to a height of 110 km, wherein the density becomes roughly constant. For $h<110$ km, the main ionic species are O_2^+, N_2^+, and NO^+. From [18], $\nu_{eg}\sim5\times10^2-5\times10^5$ s^{-1} and $\nu_{ig}\sim10-10^4$ s^{-1}. The magnetic field in the ionosphere has strength $B\sim1$ G. This implies an ion cyclotron frequency (with ion mass $m_i\approx29\,m_p$) $\omega_{ci}\sim300$ s^{-1} and an electron cyclotron frequency $\omega_{ce}\sim2\times10^7$ s^{-1}. Thus, within the lowest layers of the ionosphere, $h<110$ km, $\omega_{ci}\ll\nu_{ig}$ and we can consider Hall effects. Magnetic rotation is already seen in whistlers in Earth's ionosphere. However, we may also observe whistler drift phenomena

along the equator, where pressure gradients are normal to the direction of the dipolar magnetic field.

C. Physical Regimes of Dusty Plasmas

Approximately 1% of the baryonic matter in our galaxy is composed of dust[19]. A recent paper by Rudakov[9] on Hall plasmas in astrophysics shows how to apply the results of electron-ion Hall plasmas to dusty plasmas, in which the electron and ion plasmas are magnetized but the dust (whether through long dust gyroperiod or through collisional coupling with interstellar gas) is not:

$$\begin{aligned} &n \rightarrow n_d \\ &e \rightarrow e z_d \\ &v_i \rightarrow v_d \\ &\mathcal{D}_m \rightarrow \mathcal{D}_{m,i} = \frac{\nu_{ig} m_d c^2}{4\pi e^2 n_i \left(z_d n_d / n_i\right)^2} \end{aligned} \tag{10}$$

Where n_d and m_d are the number density and mass of dust particles (of a single mass and size), z_d is charge per dust particle, and v_d is the velocity of the dust. In the limit of low temperature plasmas ($T \lesssim 100$ K), $z_d = -1$. Dusty plasma behaves as a Hall plasma if $n_d/n_i \gg \nu_{ig}/\omega_{ci}$ [9]. The dust inertial scale, the lower limit over which we may apply Hall physics, is $\left(M_d c^2/4\pi e^2 n_d z_d^2\right)^{1/2} = c/\omega_{pd}$, where ω_{pd} is the dust plasma frequency.

In the limit that the Lorentz force on a dust particle ($ev_d B/c$) is smaller than the drag force acting on the dust ($a^2 v_{g,th} m_g n_g v_d$, where a is the size of a dust grain):

$$\frac{eB}{m_g c} < a^2 v_g n_g \tag{11}$$

Then the dust is collisionally coupled to the gas. In this limit, the dusty plasma Hall length scale c/ω_{pd} increases by a factor $\left(\mu/m_d\right)^{1/2}\left(n_g/n_d\right)^{1/2}$, similar to the length scale of the low-ionized gas in Eq. (7).

Dense molecular clouds have a hydrogen gas density of $n_H \sim 10^3 - 10^6$ cm^{-3} (see, e.g. [19, 20]). Given a standard cosmic ray ionization $\zeta = 10^{-17}$ s^{-1} [15] at temperature $T = 30$ K, this implies an ion density $n_i \sim 10^{-3} - 10^{-2}$ cm^{-3}[16, 17]. For these gas densities, the magnetic fields are on the order of $10^{-5} - 10^{-3}$ G [13, 19]. For a representative molecular cloud density $n_g = 10^3$ cm^{-3} at $T = 10$ K with representative grains of size $a = 0.03\,\mu$m, we get densities [16] $n_e = n_i = 10^{-3}$ cm^{-3}, $n_d = 10^{-8}$ cm^{-3}, and magnetic fields $B = 10^{-4}$ G. Assuming densities of dust at 3 gm/cm^3, this gives an average dust mass $m_d = 0.5 \times 10^{-15}$ gm. Furthermore, the length scale of Hall phenomena is $\left(M_d c^2/4\pi e^2 n_d z_d^2\right)^{1/2} = c/\omega_{pd} \sim$ 1000 AU.

Although the density and temperature model inside protostellar disks is still open to question, we have somewhat better estimates of the density of gas at the edges of protostellar disks and in protostellar jets. We are taking the grain radius of $a = 1\,\mu$m that scatters visible light efficiently. Since we have marginal extinction due to the scattering of light by the dust, $R n_d a^2 \sim 1$ and so $n_d \sim 3 \times 10^{-7}$ cm^{-3}. The length scale for Hall phenomena calculated over this mass and density is $c/\omega_{pd} \sim 1000$ AU. However, this length scale is smaller than that calculated because the Hall physics is defined by smaller dust particles. The usual dust size distribution function is $n_d(a) \propto a^{-3.5}$, and the length scale c/ω_{pd} changes as a^3.

II. HALL DYNAMIC EQUATIONS

First, we consider the electron-ion Hall plasma , using a cylindrical geometry and fluid equation for electrons. The Hall dynamic equations in this form were first written in [21]. Here, we begin with the Hall frozen-in equations, Eq. (5) with magnetic diffusion expression $\mathcal{D}_m$ in Eq. (6), and considering fixed ions:

$$\begin{aligned} &n \frac{\partial}{\partial t}\left(\frac{\mathbf{B}}{n}\right) + n\mathbf{v}_e \cdot \nabla\left(\frac{\mathbf{B}}{n}\right) = \left(\mathbf{B}\cdot\nabla\right)\mathbf{v}_e - \\ &\nabla\mathcal{D}_m \times \left(\nabla \times \mathbf{B}\right) + \mathcal{D}_m \nabla^2 \mathbf{B} \\ &\nabla \times \mathbf{B} = \frac{4\pi}{c}\mathbf{J} = \frac{4\pi e n}{c}\mathbf{v}_e \end{aligned} \tag{12}$$

We consider an axisymmetric magnetic field in cylindrical geometry. Only two variables completely describe the axisymmetric magnetic field: 1) the axisymmetric toroidal magnetic field $B \equiv B_\phi$; and 2) the axisymmetric toroidal vector potential $A \equiv A_\phi$. This implies the following expression for the three-component (poloidal and toroidal magnetic field):

$$\begin{aligned} &\mathbf{B} = B\mathbf{e}_\phi + \nabla \times \left(A\mathbf{e}_\phi\right) \\ &B_r = \left[\nabla \times \left(A\mathbf{e}_\phi\right)\right]_r = -\frac{\partial A}{\partial z} \\ &B_z = \left[\nabla \times \left(A\mathbf{e}_\phi\right)\right]_z = \frac{1}{r}\frac{\partial (rA)}{\partial r} \\ &B_\phi = B \end{aligned} \tag{13}$$

Where B_r and B_z are the radial and vertical components of the poloidal magnetic field, and B_ϕ is the toroidal component. Note that the expressions for magnetic field are commonly used in tokamak physics and other axisymmetric MHD problems.

Second, we get the following electron velocity:

$$\begin{aligned} &\mathbf{v}_e = -\frac{c}{4\pi e n}\nabla \times \mathbf{B} \\ &v_e^r = -\frac{c}{4\pi e n}\left[\nabla \times \left(B\mathbf{e}_\phi\right)\right]_r = \frac{c}{4\pi e n}\frac{\partial B}{\partial z} \\ &v_e^z = -\frac{c}{4\pi e n}\left[\nabla \times \left(B\mathbf{e}_\phi\right)\right]_z = -\frac{c}{4\pi e n r}\frac{\partial (rB)}{\partial r} \\ &v_e^\phi = -\frac{c}{4\pi e n}\left[\nabla \times \left(\nabla \times \left(A\mathbf{e}_\phi\right)\right)\right]_\phi \\ &\quad = \frac{c}{4\pi e n}\left(\frac{1}{r}\frac{\partial}{\partial r}\left(r\frac{\partial A}{\partial r}\right) - \frac{A}{r^2} + \frac{\partial^2 A}{\partial z^2}\right) \end{aligned} \tag{14}$$

Where v_e^r, v_e^z, and v_e^ϕ are the radial, vertical, and azimuthal components of the electron flow velocity, respectively. With Eq. (14), the continuity equation for the electron fluid, and Maxwell's equations, the plasma number density is steady-state $\partial n/\partial t = 0$.

A. Hall Dynamic Equations

Let $\mathcal{D}_m$ be a constant. Employing Eq. (13) and Eq. (14) we get the following sets of equations:

$$\begin{aligned}\frac{\partial B}{\partial t} =& -\left(\frac{\partial\left(rB\right)}{\partial z}\frac{\partial}{\partial r}-\frac{\partial\left(rB\right)}{\partial r}\frac{\partial}{\partial z}\right)\frac{B}{nr}+\\ &\mathcal{D}_m\left(\frac{1}{r}\frac{\partial}{\partial r}\left(r\frac{\partial B}{\partial r}\right)-\frac{B}{r^2}+\frac{\partial^2 B}{\partial z^2}\right)-\\ &\left(\frac{\partial\left(rA\right)}{\partial z}\frac{\partial}{\partial r}-\frac{\partial\left(rA\right)}{\partial r}\frac{\partial}{\partial z}\right)\\ &\frac{1}{nr}\left(\frac{1}{r}\frac{\partial}{\partial r}\left(r\frac{\partial A}{\partial r}\right)-\frac{A}{r^2}+\frac{\partial^2 A}{\partial z^2}\right)\end{aligned} \tag{15}$$

$$\begin{aligned}\frac{\partial A}{\partial t} =& -\frac{1}{nr^2}\left(\frac{\partial\left(rB\right)}{\partial z}\frac{\partial}{\partial r}-\frac{\partial\left(rB\right)}{\partial r}\frac{\partial}{\partial z}\right)rA+\\ &\mathcal{D}_m\left(\frac{1}{r}\frac{\partial}{\partial r}\left(r\frac{\partial A}{\partial r}\right)-\frac{A}{r^2}+\frac{\partial^2 A}{\partial z^2}\right)\end{aligned} \tag{16}$$

If we make the following sets of normalizations of time, space, magnetic field, density, velocity, and magnetic diffusion $\mathcal{D}_m$ as shown below:

$$\begin{array}{ll} t\rightarrow t\omega_{ci} & (r,z)\rightarrow(r,z)\omega_{pi}/c \\ B\rightarrow B/B_0 & A\rightarrow A/A_0 = A\omega_{pi}/\left(cB_0\right) \\ n\rightarrow n/n_0 & \omega_{ci} = eB_0/m_i c \\ \omega_{pi}^2 = 4\pi e^2 n_0/m_i & v\rightarrow v/v_A \\ \mathcal{D}_m\rightarrow\nu_{ei}/\omega_{ce} & v_A = B_0/\sqrt{4\pi n_0 m_i} \\ \omega_{ce} = eB_0/m_e c & \end{array} \tag{17}$$

Where B_0 and n_0 are the maximum toroidal magnetic field (or magnetic field strength) and number density, respectively. ω_{ce}, ω_{ci}, ω_{pi}, v_A, are the electron cyclotron frequency, ion cyclotron frequency, ion plasma frequency, and Alfvén velocity at that point, respecively.

Typically in magnetohydrodynamics, for axisymmetric configurations only the resistive term in Eq. (16) exists. According to Cowling's anti-dynamo theorem (see, e.g. [22, 23]), at late times there is no poloidal magnetic field in an axisymmetric MHD since $A\rightarrow 0$ due to the resistive term. However, in Hall MHD, since the magnetic field is no longer tied to the bulk plasma, there appears a convective and magnetic rotational term in Eq. (16) that allows for an axisymmetric poloidal field.

B. Generalized Grad-Shafranov (GGS) Integral

Here, we show an important integral of the Hall dynamic equations. We assume propagating solutions $A\equiv A(r,z-ut)$ and $B\equiv B(r,z-ut)$, where u is a constant normalized velocity, and a radial-dependent number density $n\equiv n(r)$.

Consider force balance equation in some *moving* frame in which the electric $\mathbf{E}'$ and magnetic $\mathbf{B}'$ fields are stationary in time. Electron gas pressure and resistivity are ignored. The electron velocity in a dimensionless form, using Eq. (13), is given by:

$$\begin{aligned}\mathbf{v}_e =& -\frac{1}{n}\nabla\times\mathbf{B}\\ =& -\frac{1}{nr}\frac{\partial(rB)}{\partial r}\mathbf{e}_z+\frac{1}{n}\frac{\partial B}{\partial z}\mathbf{e}_r+\\ &\frac{1}{n}\left(\frac{1}{r}\frac{\partial}{\partial r}\left(r\frac{\partial A}{\partial r}\right)-\frac{A}{r^2}+\frac{\partial^2 A}{\partial z^2}\right)\mathbf{e}_\phi\end{aligned} \tag{18}$$

Begin with the dimensionless frozen-in law for the electron fluid neglecting electron pressure:

$$\mathbf{E}+\mathbf{v}_e\times\mathbf{B}=\mathbf{0} \tag{19}$$

The propagating solution is moving with sufficiently small velocity to ignore relativisitic effects so that:

$$\mathbf{E}'=\mathbf{E}+\mathbf{u}\times\mathbf{B},\quad \mathbf{B}'=\mathbf{B} \tag{20}$$

In this comoving frame the electric field $\mathbf{E}'=\mathbf{0}$, since electrostatic potentials are neglected. In the laboratory frame the electric field is given by:

$$\mathbf{E}=-\mathbf{u}\times\mathbf{B} \tag{21}$$

As a result, Eq. (19) can be rewritten as:

$$\left(\mathbf{v}_e-\mathbf{u}\right)\times\mathbf{B}=\mathbf{0} \tag{22}$$

A general case reproduces the generalized Grad-Shafranov (GGS) integrals with force balance in r, z, and ϕ directions in Eq. (22). Sufficiently, force balance in the radial direction implies:

$$\begin{aligned}&\left(\frac{1}{r}\frac{\partial}{\partial r}\left(r\frac{\partial A}{\partial r}\right)-\frac{A}{r^2}+\frac{\partial^2 A}{\partial z^2}\right)B_z+\\ &B\left(nu+\frac{1}{r}\frac{\partial(rB)}{\partial r}\right)=0\end{aligned} \tag{23}$$

Combined with the fact that the solution consists of magnetic surfaces at constant poloidal flux $\Psi = rA$, and that fact that $\partial H/\partial r = dH/d\Psi\times\partial\Psi/\partial r$, imply the GGS integrals.

$$\begin{aligned}&r\frac{\partial}{\partial r}\left(\frac{1}{r}\frac{\partial\Psi}{\partial r}\right)+\frac{\partial^2\Psi}{\partial z^2}=\\ &-\frac{dH}{d\Psi}\left(H(\Psi)-u\int_0^r n\left(r'\right)r'\,dr'\right)\end{aligned} \tag{24}$$

$$rB = H\left(\Psi\right)-u\int_0^r n\left(r'\right)r'\,dr' \tag{25}$$

The first current term $H(\Psi)$ arises in the normal Grad-Shafranov equation. The additional term in the GGS arises due to the electric field (see Eq. [22]) acting on the moving structure. This looks like an additional poloidal

current, $-u\int_0^r n\,(r')\,r'\,dr'$, in the frame of the propagating solution, where the motionless ions are seen moving with velocity $-u\mathbf{e}_z$. This "current" can appear only where the electrons are moving. Furthermore, radial electric force or $\mathbf{J}\times\mathbf{B}$ force due to this "current" results in a pressure term $-u\int_0^r n\,(r')\,r'\,dr'\times dH/d\Psi$ in the GGS equation. It is necessary to mention that in MHD the magnetic field is frozen into the plasma and cannot move relative to the ions, so there is no additional force. The GGS equations were first found in [21] as exact solutions of the dynamic equations for the Hall magnetic field in an axisymmetric geometry, Eq. (15) and (16).

III. ELECTRICAL JETS

Here, we consider solutions of electrical jets. We have two analytic solutions – one for the GGS equation with linear current term $H(\Psi)\propto\Psi$, and the resistive nonlinear shock which propagates as Burgers equation – and numerical estimates, with justification on the basis of the Chandrasekhar-Fermi theorem[24], of nonlinear solitons in the GGS integral. According to this theorem, it was shown in an MHD plasma that a localized equilibrium plasma magnetic structure could exist only in the presence of an external magnetic field or with fixed metal wall boundaries.

A. Resistive Nonlinear Shock

Again, assume a Hall plasma column, so that our magnetic fields are given by Eq. (16) and (15), with a constant-density plasma within the column $r<R$ and vacuum outside. Furthermore, let us assume only the toroidal field B exists with profile $B(r,z,t)=B(z,t)r/R$ and $B(-\infty,t)=-B_0$, where $B_0>0$. Thus, we get the following Burger's equation in normalized coordinates:

$$\frac{\partial B}{\partial t}=\frac{2B}{R}\frac{\partial B}{\partial z}+\mathcal{D}_m\frac{\partial^2 B}{\partial z^2} \tag{26}$$

With the following solution, in normalized coordinates:

$$B(r,z,t)=\begin{cases}\dfrac{B_0 r}{2R}\left(\tanh\left(\dfrac{B_0\,(z-B_0t/R)}{2R\mathcal{D}_m}\right)-1\right) & r<R\\ 0 & r>R\end{cases} \tag{27}$$

So that in dimensional values the shock velocity is given by $u=cB_0/\left(4\pi enR\right)$ and shock thickness $\delta=2\nu_{ei}/\omega_{ce}R$. Note that the shock is moving in the positive z direction in our coordinate system; this asymmetry is typical for Hall phenomena. Furthermore, one may construct analytic solutions for any arbitrary initial configuration $B(z,0)$ (see e.g. [4, 25] for the Hopf-Cole transformation hat transforms Burger's equation into a heat diffusion equation). A plot of the toroidal magnetic structure of this resistive case is shown in figure 1, with $u=100$ and $b_0=B_0/R=100$.

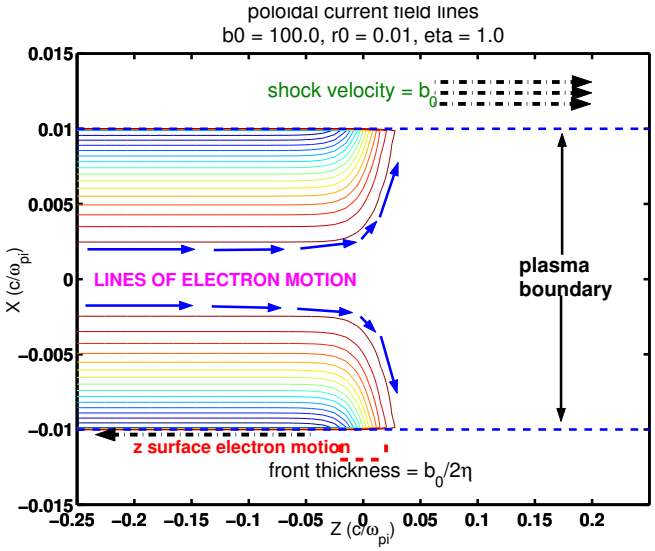

FIG. 1: Poloidal current lines within the Burgers-like nonlinear solution. Here, electrons must return across the surface so, we see that a current sheet develops on the Hall plasma column, that distributes current back into the (attached) current generator.

Here a more general argument for Hall propagation, where the ions are motionless, is given. Consider the dynamics of a magnetic field located in a long Hall plasma cylinder of axial length $L_{\max}$ and fixed radius R that consists of a constant density n. Initially, the magnetic field has toroidal profile $B=-B_0r/R$ (where $B_0>0$) and is localized within some axial length $0\le z\le L_0$, where $L_0<L_{\max}$, and there is no magnetic field at $z>L_0$. A metal divider at $z=L_0$ prevents the propagation of the magnetic field. There are no additional sources of current and magnetic field into this closed system. If the radius is much larger than the electron collisional skin depth, then magnetic flux must be conserved.

Then the sheet is removed on time scales much smaller than R/u, where u is the velocity of Hall shock propagation, so that we get negligibly changing magnetic fields and negligible electric fields and "arcing" in the removal of the divider. The cylinder, and the process described here, is shown in figure 2. In calculating the magnetic fluxes, we integrate over the bottom half of the surface in the penetrating volume in figure 2.

Within some small time Δt such that $\Delta L=u\Delta t\ll L_0$, the magnetic field amplitude and currents entering this small volume ΔL do not change. The electrons that flow in axially into the Hall plasma column (into the unmagnetized volume) must balance the electrons flowing in a skin layer along the vacuum boundary of the plasma column. There is a corresponding flow of magnetic field in the bulk plasma with the electrons and out along the vacuum boundary. The rate of inflow of magnetic flux

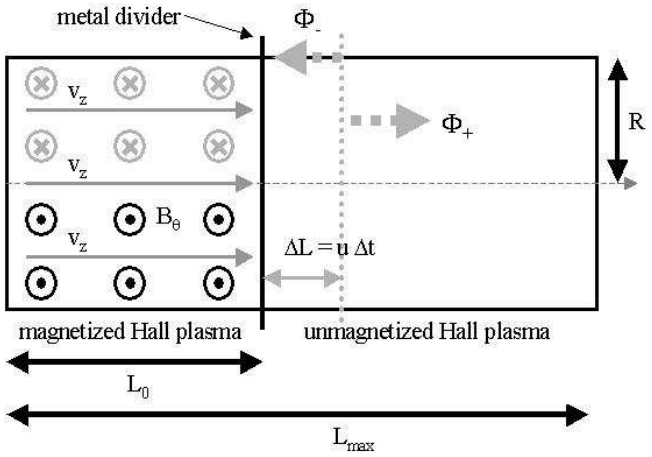

FIG. 2: Cartoon depicting the closed cylindrical box, within which a Hall plasma resides. Flux is conserved due to the fact that the radius is much larger than the electron collisional skin depth, and initially the Hall plasma is separated into unmagnetized and magnetized (with toroidal magnetic profile $B \propto r$) regions by a metal divider. When the divider is removed, magnetic fields propagate with some shock velocity u. v_z denotes the electron velocity.

through the Hall column into the volume $z > L_0$:

$$\begin{aligned}\dot{\Phi}_+ =& \int_R^0 v_z B\, dr \\ =& \frac{c}{4\pi e}\int_0^R \frac{B}{nr}\frac{\partial (rB)}{\partial r}\, dr = \frac{cB_0^2}{4\pi en}\end{aligned} \tag{28}$$

And the flow of magnetic flux out of the plasma column through a surrface skin layer of width $\Delta R \ll R$:

$$\begin{aligned}\dot{\Phi}_- =& \int_R^{R-\Delta R} v_z B\, dr \\ =& \frac{1}{8\pi en}\int_{R-\Delta R}^R \frac{\partial B^2}{\partial r}\, dr = -\frac{cB_0^2}{8\pi en}\end{aligned} \tag{29}$$

From Eq. (28) and (29) the flux inflow rate into the volume is twice that of the flux outflow rate, so that there is a net magnetic flux flow which is seen as a Hall shock wave. The structure moves with a Hall shock velocity u, so that the net change in flux within the column:

$$\begin{aligned}\dot{\Phi}_{\rm net} =& u\int_0^R B_0\,(r/R)\, dr \\ =& \frac{1}{2}uB_0R = \dot{\Phi}_+ + \dot{\Phi}_- = \frac{cB_0^2}{8\pi en}\end{aligned} \tag{30}$$

One gets the general calculated shock Hall velocity, $u = cB_0/\left(4\pi enR\right)$, from the flux balance equation.

Second, we show that magnetic energy dissipation is a natural consequence of this system. At late times, the magnetic field propagates to a length $L_{\rm max} > L_0$ and equilibrates with amplitude B_f and uniform structure in z. Flux conservation of the toroidal B field in an rz flux surface over the bottom half, where $0 \le r \le R$, $0 \le z \le L(t)$:

$$B_0L_0 = B_fL_{\rm max} \tag{31}$$

Now we calculate the final magnetic energy $\mathcal{E}_f$, where the initial magnetic energy $\mathcal{E}_0$.

$$\begin{aligned}\mathcal{E}_f =& 2\pi\int_0^R r\, dr\int_0^{L_{\rm max}} \frac{B_f^2\,(r/R)^2}{8\pi} \\ =& \mathcal{E}_0\left(\frac{L_0}{L_{\rm max}}\right)^2\frac{L_{\rm max}}{L_0} = \mathcal{E}_0\frac{L_0}{L_{\rm max}}\end{aligned} \tag{32}$$

Which implies the existence of some dissipative mechanism – either through electron collisionality [1] or through ion inertia [2], for example – during magnetic field propagation through a Hall plasma.

B. Periodic GGS Solution

Here, we consider solutions to the GGS equation (see Eq. [25] and [24]) with linear current terms, $H(\Psi) = k\Psi$. Note that this solution arises from a particular choice of current term, and does not arise from a linearization of the dynamic equations (Eq. [16] and [15]). Consider the density $n = 1$ a constant, and as before $u > 0$ is also a constant. Then the GGS integrals reduce to the following inside the plasma column of radius R:

$$r\frac{\partial}{\partial r}\left(\frac{1}{r}\frac{\partial\Psi}{\partial r}\right) + \frac{\partial^2\Psi}{\partial z^2} = -k^2\Psi + \frac{1}{2}ukr^2 \tag{33}$$

$$B = kA - \frac{1}{2}ur^2 \tag{34}$$

Outside the plasma column we have a vacuum, so that there are no currents and no magnetic field in the frame of electron MHD. Electron MHD implies that the magnetic field is carried only by the electrons.

We consider a geometry in which there is a given radial variation in the three-component magnetic field, such that there is only a toroidal current sheet. This implies that $B \to 0$ at the boundary of the plasma column. We look for solutions that go as $\sim \cos\kappa\,(z - ut)$ in magnetic field.

$$\begin{aligned}\Psi =& \begin{cases}\alpha r J_1\left(r\sqrt{k^2-\kappa^2}\right)\cos\kappa\,(z-ut) + \frac{ur^2}{\kappa} & r < R \\ \frac{uR^2}{k} & r > R\end{cases} \\ B =& \begin{cases}\kappa\alpha J_1\left(r\sqrt{\kappa^2-k^2}\right)\cos k\,(z-ut) & r < R \\ 0 & r > R\end{cases}\end{aligned} \tag{35}$$

Where J_n are Bessel functions, $\kappa^2 > k^2$, and the condition that $J_1\left(R\sqrt{\kappa^2-k^2}\right) = 0$. The toroidal surface current on the plasma column is given by:

$$\begin{aligned}I_\phi\,(R, z-ut) =& \alpha\sqrt{\kappa^2-k^2}\left(J_0\left(R\sqrt{\kappa^2-k^2}\right) - \right. \\ & \left. J_2\left(R\sqrt{\kappa^2-k^2}\right)\right)\cos k\,(z-ut) + \frac{2u}{\kappa}\end{aligned} \tag{36}$$

The solution shown in figures 3, with the following parameters:

$$\eta = 0.0 \quad \alpha = 1.0$$
$$\kappa = 1.0 \quad u = 100.0$$

And κ given by the first zero of $J_1(x)$:

$$k = \sqrt{\kappa^2 + \left(\frac{3.83171}{R}\right)^2}$$

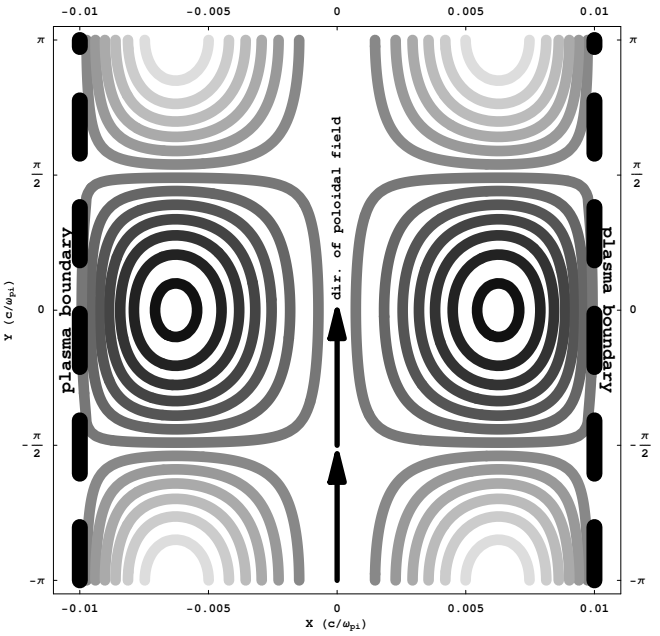

FIG. 3: Poloidal magnetic flux Ψ (and hence, poloidal magnetic field lines) for the GGS solution. Note that since the poloidal flux within the vacuum is constant, no poloidal magnetic fields exist within the vacuum. Note that the discontinuity in B_z results in ϕ current sheet along the Hall column surface. This magnetic configuration appears similar to the compact torus, where the structure is defined by the boundary conditions – i.e. metal walls.

C. Soliton-Like Solutions

Here, we consider solutions to the GGS equation that describes the evolution of possible 2D nonlinear whistler-like waves and structures. Consider solutions with normalized density $n = 1$, solutions propagating with velocity $u\mathbf{e}_z$, and the following currents and toroidal magnetic fields in the GGS integral:

$$\begin{aligned} &H(\Psi) = \alpha\Psi^2 \\ &rB = H(\Psi) - \frac{1}{2}ur^2 = \alpha\Psi^2 - \frac{1}{2}ur^2 \end{aligned} \tag{37}$$

n terms of the toroidal vector potential A and the toroidal magnetic field B the nonlinear soliton equation is given by the following:

$$\begin{aligned} &\frac{\partial^2 A}{\partial r^2} + \frac{1}{r}\frac{\partial A}{\partial r} - \frac{A}{r^2} - ur^2 A + 2r^2\alpha A^3 = 0 \\ &B = \alpha r A^2 - \frac{1}{2}ur \end{aligned} \tag{38}$$

One can easily show that if we let $A_0(r,z)$ be the solution to the following differential equation, $u = 1, \alpha = 1$:

$$\frac{\partial^2 A_0}{\partial r^2} + \frac{1}{r}\frac{\partial A_0}{\partial r} - \frac{A_0}{r^2} - r^2 A_0 + 2r^2 A_0^3 = 0 \tag{39}$$

Then the following scaling for the toroidal vector potential $A(r,z;u,\alpha)$ in terms of $A_0(r,z)$ and the form of the toroidal magnetic field from Eq. (38) are given by:

$$A(r,z;\mu,\alpha) = \left(\frac{\alpha}{u}\right)^{1/2} A_0\left(u^{1/4}r, u^{1/4}z\right) \tag{40}$$

$$B(r,z;u,\alpha) = \left(\frac{\alpha}{u}\right)^{3/2} rA_0\left(u^{1/4}r, u^{1/4}z\right)^3 - \frac{1}{2}ur \tag{41}$$

Consider a volume to be a cylinder. The soliton structure consists of a three-component magnetic field (a poloidal field and a toroidal field) that is localized about the origin with a span much smaller than the dimensions of the cylindrical volume; thus, $B_r \to 0$, $B_z \to 0$, and $B_\phi \to -\frac{1}{2}ur$ at the boundaries of the cylinder. Employing the Chandrasekhar-Fermi theorem – using $\mathbf{r}\cdot(\mathbf{J}\times\mathbf{B})$ force balance within the cylindrical volume – one can show the following:

$$\begin{aligned} &\int_{r=0}^{R}\int_{z=-L}^{L} rB_z^2\, dr\, dz = \\ &\int_{r=0}^{R}\int_{z=-L}^{L} un(r)rH(\Psi)\, dr\, dz \end{aligned} \tag{42}$$

Furthermore, since $B_z = -\partial A/\partial r$, a localized solution (where the integral on the left hand side is finite) is possible provided that the right hand side ≥ 0. To guarantee a localized solution we require that $H(\Psi) \geq 0$. The case analyzed in this section is $H(\Psi) = \Psi^2 \geq 0$.

Note that the form of Eq. (38) or (39) is as if we consider a nonlinear 3D Schrödinger equation with the $m = 1$ azimuthal modes (i.e. solutions $\sim e^{i\phi}$). Here, to estimate the form of the soliton, we use the same variational method and trial functions, described below, for 3D nonlinear optical solitons [26]. First, we derive the Lagrangian that describes the GGS equation with nonlinear current. Then we look for localized solutions with different test functions. One reasonable approximation for the test function in cylindrical coordinates is $A(r,z) = U(r)\,\mathrm{sech}\,\mu z$. A one-dimensional differential equation in r is derived by averaging that Lagrangian with respect to z and searching for a localized one-node solution, presumed to be the main lowest-energy stable solution, for a given μ. We solve for that μ that minimizes the integral of the averaged Lagrangian over r. Another test function is in spherical coordinates, $A(\rho,\theta) = U(\rho)\sin\theta$, where $\rho = \sqrt{r^2+z^2}$ and $\cos\theta = z/\rho$. Again a one-dimensional

equation in ρ, and its localized single-node lowest energy solution, is derived by averaging and minimizing the Lagrangian of the GGS. A more detailed description of the estimation method for both trial functions is provided in the Appendix.

Plots of the dependence $U(r)$, the cylindrical ansatz, and $U(\rho)$, the spherical ansatz, are shown in figure 4. Contours detailing the shapes of the toroidal vector potential $A(r,z)$ for both trial functions are shown in figure 5. The cylindrical ansatz $U(r)\,\mathrm{sech}\,\mu z$ and the spherical ansatz $U(\rho)\sin\theta$ have approximate shapes in the radial coordinate. As in [26], there is a substantial differences in the shape of the cylindrical and spherical trial functions of the soliton. The shape of the cylindrical and spherical trial functions look similar to their corresponding solutions of the optical solitons found in [26]. Both trial functions also satisfy the scaling $A\left(r,z;\mu,\alpha\right) = \left(\alpha/u\right)^{1/2} A_0\left(u^{1/4}r, u^{1/4}z\right)$.

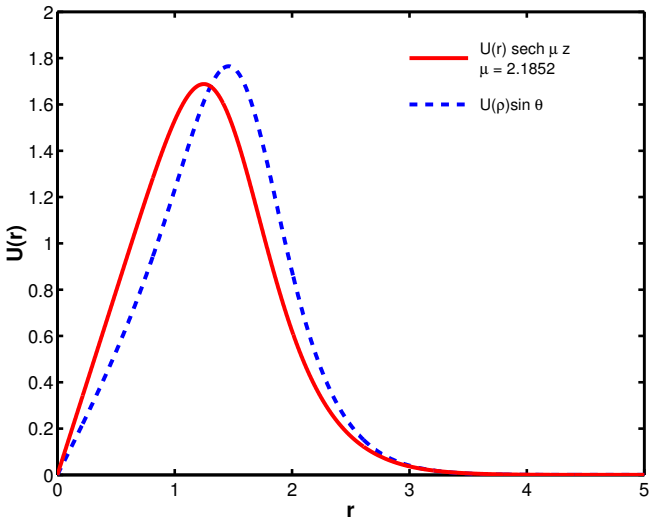

FIG. 4: Plot of the radial distribution with the given ansatzes shown in the figure. For the cylindrical ansatzes, the z width parameter μ is calculated to four decimal places.

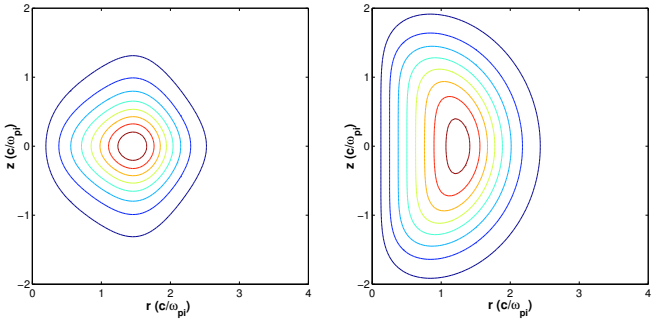

FIG. 5: Structure of the $U(r)\mathrm{sech}\,\mu z$ ansatz (left) compared with the spherical $U(\rho)\sin\theta$ ansatz (right). Although the finer features are obviously different, the width in the radial direction are roughly similar.

IV. DISCUSSION AND CONCLUSIONS

Here we have explored possible structures that arise in a Hall plasma due to curvature rather than, say, density gradients. We have provided a general structure to continue further analysis of the dynamic axisymmetric Hall modes in Eq. (15) and (16) as well as the generalized Grad-Shafranov (GGS) integrals in Eq. (24) and (25) and propagating solutions with constant velocities in the z direction.

Well-understood Hall plasma phenomena such as whistler drift modes were shown to exist in an homogenous cylindrical plasma column. Furthermore, an exact solution for the whistler drift mode, the Burgers nonlinear shock wave, was discussed in subsection III A.

Periodic solutions were shown in subsection III B from a simple analysis of the allowable solution for linear current in the GGS integrals. We find that the solution is constrained by the radial vacuum boundary of a Hall plasma column, because in Hall physics the magnetic field is carried solely by the electrons. Further work may involve a search for transitional solutions – those solutions intermediate between the periodic Grad-Shafranov solution and the collisional nonlinear shock. Possible solutions may be those with oscillatory substructure in the toroidal magnetic field at the shock with corresponding poloidal magnetic field in the case of small resistivity.

We found that there is a similarity between the GGS and the nonlinear Schrödinger equation with $m = 1$ azimuthal modes. We apply the variational method, which was developed for optical fiber solitons, for our problem. We estimate soliton solutions in subsection III C for a given nonlinear current $H(\Psi) = \alpha\Psi^2$ and constant number density n. The Chandrasekhar-Fermi theorem implies that such a nonlinear current may allow for localized soliton solutions. Such a current distribution also allows for a simple scaling – that is, solutions with normalized propagation velocity $u \neq 1$ and current scalings $\alpha \neq 1$, and $u > 1, \alpha > 1$ have vector potential $A\left(r,z;u,\alpha\right) = \left(\alpha/u\right)^{1/2} A_0\left(u^{1/4}r, u^{1/4}z\right)$. Further research may apply this suggested method to other localized soliton-like solutions. The Hall dynamic equations in Eq. (15) and (16) may be useful in analyzing the stability of the soliton solutions estimated here.

We have also included some space plasmas in which the Hall regime may be important. In Earth's lower ionosphere, whistler drift modes due to density gradients (at the equator) or curvature (at the magnetic poles) may exist. In astrophysical plasmas, such as molecular clouds, protostellar disks, or protostellar jets, Hall phenomena may exist due to the presence of charged dust. Furthermore, some groups in the ionosphere community have begun using 2D and 3D Hall MHD codes [5, 27], to which our analytic results could provide a first step to explore astrophysical Hall phenomena.

Axisymmetric Hall phenomena may play an important role in the circumstellar disks and jets pictured by the Hubble Space Telescope around young stellar objects.

The typical circumstellar disk has a radius of a few hundred AUs – a possible length scale in Hall phenomena. Hall shocks and other magnetic structures also transport of currents and magnetic fields through matter without compression or net mass motion. A comparison of the radio frequency Doppler studies of the bipolar jets around HH30 show that the bulk velocity of the matter is five times slower than the velocities of the observed jet substructures [28]. Furthermore, radio polarization measurements of the jets emanating from the disks of GM Aurigae and DG Tauri imply largely toroidal magnetic fields[29], which may be explainable as a nonlinear shock wave and structures rather than the traditional model of a supersonic fluid or MHD shock.

Other explanations for the fast-moving, time-resolved substructures in the jets of T Tauri stars involve "bullets" of plasma that emanate from the disk [30]. Furthermore, a variety of MHD jet models are given in the literature (see, e.g. [30–32]). Here, due to the obvious presence of dust, we imply a very different model, magnetic penetration into a Hall plasma, that may explain some of these structures.

Acknowledgments

The authors would like to thank Prof. B. Coppi for his helpful advice. L. Rudakov has been supported through a Department of Energy grant through Massachusetts Institute of Technology. T. Islam has been supported through Department of Energy Grant #AAA-999.

[1] A. S. Kingsep, Y. V. Mokhov, and K. V. Chukbar, Fiz. Plazmy **10**, 854 (1984).
[2] A. Fruchtman and L. Rudakov, Phys. Rev. Lett. **69**, 2070 (1992).
[3] J. D. Huba, I. M. Grossman, and P. F. Ottinger, Phys. Plasmas **1**, 3444 (1994).
[4] A. V. Gordeev, A. S. Kingsep, and L. I. Rudakov, Physics Reports **243**, 214 (1994).
[5] J. D. Huba, Phys. Plasmas **2**, 2504 (1995).
[6] L. I. Rudakov, Phys. Plasmas **283**, 177 (1997).
[7] M. A. Shay, J. F. Drake, R. E. Denton, and D. J. Biskamp, J. Geophys. Res. **103**, 9165 (1998).
[8] S. A. Balbus and C. Terquem, Astrophys. J. **552**, 235 (2001).
[9] L. I. Rudakov, Phys. Scripta **T89**, 158 (2001).
[10] B. T. Draine, W. G. Roberge, and A. Dalgarno, Astrophys. J. **264**, 485 (1983).
[11] S. Chapman, Nuovo Cimento **5**, 1385 (1956).
[12] S. Frómang, C. Terquem, and S. A. Balbus, Mon. Not. R. Astron. Soc. **329**, 18 (2002).
[13] P. C. Myers and A. A. Goodman, Astrophys. J. **326**, L27 (1988).
[14] M. Oppenheimer and A. Dalgarno, Astrophys. J. **192**, 29 (1974).
[15] L. Spitzer and M. G. Tomasko, Astrophys. J. **152**, 971 (1968).
[16] T. Umebayashi and T. Nakano, Mon. Not. R. Astron. Soc. **243**, 236 (1990).
[17] M. Wardle and C. Ng, Mon. Not. R. Astron. Soc. **303**, 239 (1999).
[18] F. S. Johnson, ed., *Satellite Environment Handbook* (Stanford Univ. Press, Stanford, CA, 1961).
[19] E. G. Zweibel, Phys. Plasmas **6**, 1725 (1999).
[20] T. W. Harquist, W. Pilipp, and O. Havnes, Astrophysics and Space Science **246**, 243 (1997).
[21] L. I. Rudakov, Phys. Scripta **T98**, 58 (2002).
[22] T. G. Cowling, Mon. Not. R. Astron. Soc. **94**, 2 (1934).
[23] P. M. Bellan, *Spheromaks: a Practical Application of Magnetohydrodynamic Dynamos and Plasma Self-Organization* (Imperial Press College, 2000).
[24] S. Chandrasekhar and E. Fermi, Astrophys. J. **118**, 116C (1953).
[25] S. I. Vainshtein, S. M. Chitre, and A. V. Olinto, Phys. Rev. E **61**, 4422 (2000).
[26] A. Desyatnikov, A. Maimistov, and B. Malomed, Phys. Rev. E **61**, 3107 (2000).
[27] J. Huba and L. I. Rudakov (2002), submitted to Phys. Rev. Lett.
[28] C. J. Lada and M. Fitch, Astrophys. J. **459**, 638 (1996).
[29] M. Tamura, G. H. Hough, J. S. Greaves, J.-I. Morino, A. Chrisostomou, W. S. Holland, and M. Momose, Astrophys. J. **525**, 832 (1999).
[30] W. I. Newman, A. L. Newman, and R. V. E. Lovelace, Astrophys. J. **392**, 622 (1992).
[31] R. V. E. Lovelace, M. M. Romanova, and G. S. Bisnovatyi-Kogan, Mon. Not. R. Astron. Soc. **275**, 244 (1992).
[32] G. V. Ustyogova, R. V. E. Lovelace, M. M. Romanova, H. Li, and S. A. Colgate, Astrophys. J. **541**, L21 (2000).

APPENDIX: VARIATIONAL METHOD FOR TRIAL FUNCTIONS OF GGS

Here, we demonstrate localized 3D soliton solutions of the GGS equation with nonlinear current term, with the cylindrical coordinate and spherical coordinate trial functions. This variational method and trial functions were borrowed from [26]. Furthermore, the integration of the one-dimensional functions was performed using a fourth-order Runge-Kutta method from $r = 0$ to $r = 10$ for the cylindrical ansatz and $\rho = 0$ to $\rho = 10$ for the spherical ansatz.

1. Cylindrical Coordinate Ansatz

The Lagrangian of the differential expression (39) is given by the following:

$$L\left(\partial_r A_0, \partial_z A_0, A_0; r, z\right) = \frac{1}{2} r \left(\partial_r A_0\right)^2 + \frac{1}{2} r \left(\partial_z A_0\right)^2 + \frac{A_0^2}{2r} + \frac{1}{2} r^3 A_0^2 - \frac{1}{2} r^3 A_0^4 \tag{A.1}$$

With the following ansatz:

$$A_0(r, z) = U(r) \operatorname{sech}(\mu z) \tag{A.2}$$

We get the following averaged Lagrangian $\mathcal{L}_1$, where $U' = dU/dr$:

$$\begin{aligned} \mathcal{L}_1 &= \int_{-\infty}^{\infty} L\left(\partial_r A_0, \partial_z A_0, A_0; r, z\right)\, dz \\ &= \frac{r}{\mu}\left(\frac{dU}{dr}\right)^2 + \frac{\mu r}{3} U^2 + \frac{U^2}{\mu r} + \frac{r^3}{\mu} U^2 - \frac{2r^3}{3\mu} U^4 \end{aligned} \tag{A.3}$$

If we vary $\mathcal{L}$ with respect to U and dU/dr we then have the following differential equation in r:

$$\frac{d^2U}{dr^2} + \frac{1}{r}\frac{dU}{dr} - \frac{U}{r^2} - \frac{1}{3}\mu^2 U - r^2 U + \frac{4}{3} r^2 U^3 = 0 \tag{A.4}$$

The solutions that we look for are given by the

$$\begin{aligned} &\lim_{r\to 0} U(r) = U'(0) r \\ &\lim_{r\to\infty} U(r) = r^{-1} \exp\left(-\frac{1}{2} r^2\right) \end{aligned} \tag{A.5}$$

We employ the shooting method, with free parameter $U'(0)$, by integrating out Eq. (A.4) from $r = 0$ to some sufficiently large $r = r_{\text{lim}} \gg w$, where w is the width of the structure. Furthermore, since we postulate the lowest-energy solutions are probably dominant, we look for solutions that have a single node in $U(r)$.

For each μ there is a unique single-node solution $U(r;\mu)$ satisfying Eq. (A.4). To solve for this problem, we require that the averaged Lagrangian Eq. (A.3), averaged over r, must be extremized with respect to μ:

$$\int_0^{\infty} \frac{\partial \mathcal{L}_1}{\partial \mu}\, dr = 0 \tag{A.6}$$

If we use the following functions:

$$\begin{aligned} \epsilon_1(\mu) &= \int_0^{\infty} r U(r;\mu)^2\, dr \\ \epsilon_2(\mu) &= \int_0^{\infty} r^3 U(r;\mu)^2\, dr \\ \epsilon_3(\mu) &= \int_0^{\infty} r^3 U(r;\mu)^4\, dr \end{aligned} \tag{A.7}$$

We then get the following relation:

$$\int_0^{\infty} r\left(\left(\frac{dU}{dr}\right)^2 + \frac{U^2}{r^2}\right) dr = \frac{1}{3}\mu^2 \epsilon_1(\mu) - \epsilon_2(\mu) + \frac{2}{3}\epsilon_3(\mu) \tag{A.8}$$

However, using (A.4) one can show the following relation:

$$r\left[\left(\frac{dU}{dr}\right)^2 + \frac{U^2}{r^2}\right] = \frac{d}{dr}\left(rU\frac{dU}{dr}\right) - \frac{1}{3}\mu^2 r U^2 - r^3 U^2 + \frac{4}{3} r^3 U^4 \tag{A.9}$$

Substituting Eq. (A.9) into the integral on the left hand side of Eq. (A.8), and noting that the first right hand side term in Eq. (A.9) integrates to zero because it is a surface term, we then get the following residual function for μ_0:

$$\delta_1(\mu_0) = \mu_0^2 \epsilon_1(\mu_0) - \epsilon_3(\mu_0) = 0 \tag{A.10}$$

Our estimates of μ_0 (to four decimal places) and U_0' that satify (A.10) are given below:

$$\begin{aligned} &\mu_0 \approx 2.1852 \\ &U'(0) \approx 1.01152274261063 \end{aligned} \tag{A.11}$$

2. Spherical Coordinate Ansatz

For the spherical coordinate ansatz, we transform (39) into spherical coordinates, with $\rho = \sqrt{r^2 + z^2}$ and $\cos\theta = z/\sqrt{r^2+z^2}$:

$$\frac{1}{\rho^2}\frac{\partial}{\partial\rho}\left(\rho^2 \frac{\partial A_0}{\partial \rho}\right) + \frac{1}{\rho^2 \sin\theta}\frac{\partial}{\partial\theta}\left(\sin\theta \frac{\partial A_0}{\partial\theta}\right) - \frac{A_0}{\rho^2 \sin^2\theta} - \rho^2 \sin^2\theta A_0 + 2\rho^2 \sin^2\theta A_0^3 = 0 \tag{A.12}$$

Which has the following Lagrangian:

$$L\left(\partial_\rho A_0, \partial_\theta A_0, A_0; \rho, \theta\right) = \frac{1}{2}\rho^2 \sin\theta \left(\frac{\partial A_0}{\partial \rho}\right)^2 + \frac{1}{2}\sin\theta\left(\frac{\partial A_0}{\partial\theta}\right)^2 + \frac{A_0^2}{2\sin\theta} + \frac{1}{2}\rho^4 \sin^3\theta A_0^2 - \frac{1}{2}\rho^4 \sin^3\theta A_0^4 \tag{A.13}$$

With the following ansatz:

$$A_0(\rho, \theta) = U(\rho)\sin\theta \tag{A.14}$$

We get the following averaged Lagrangian:

$$\begin{aligned} \mathcal{L}_2 &= \int_0^{\pi} L\left(\partial_\rho A_0, \partial_\theta A_0, A_0; \rho, \theta\right)\, d\theta \\ &= \frac{2}{3}\rho^2\left(\frac{dU}{d\rho}\right)^2 + \frac{4}{3}U^2 + \frac{8}{15}\rho^4 U^2 - \frac{16}{35}\rho^4 U^4 \end{aligned} \tag{A.15}$$

That results in the following differential expression:

$$\frac{d^2U}{d\rho^2} + \frac{2}{\rho}\frac{dU}{d\rho} - \frac{2U}{\rho^2} - \frac{4}{5}\rho^2 U + \frac{48}{35}\rho^2 U^3 = 0 \tag{A.16}$$

We shoot with $U(0) = 0$ and free parameter $U'(0)$ such that for sufficiently large ρ, we get $U(\rho) \to \alpha\rho^{-1}\exp\left(-\rho^2/5\right)$, where α is some constant. Here, we have the following $U'(0)$:

$$U'(0) \approx 1.589689693 \tag{A.17}$$